

# The Preliminary Structural and Thermal Modeling of a Small Student-Developed Liquid Rocket Engine

Austin Morse<sup>1</sup>, Zachary Moore<sup>2</sup>, Christa Cartwright<sup>3</sup>, Steven Jones<sup>4</sup>,  
Phineas Masters<sup>5</sup>, Jacob Williams<sup>6</sup>

*The University of Alabama in Huntsville, Huntsville, Alabama, 35805, USA*

Tartarus is a student-led project of the Space Hardware Club at the University of Alabama in Huntsville working to develop a small-scale liquid rocket engine. In order to characterize the engine's performance during firing and validate safety requirements, various numerical and finite element modeling methods were applied to simulate engine firing behavior. First-order performance and thermal calculations to compare higher-fidelity results against were obtained with a custom quasi-one-dimensional performance model. To model the engine's thermal and structural performance during its firing, a structural-thermal finite element analysis software was used. Additionally, CFD models were employed to model supersonic flow in the nozzle assuming both frozen and reacting flow, for comparison against 1-D performance assumptions. Multiphase simulations were also designed to model the impingement of the propellant streams and cooling performance of the boundary layer cooling system. Through this preliminary work, the team aims to begin development of a full multiphysics model of propellant injection, combustion, and flow.

## I. Introduction

The Tartarus project is a project of The University of Alabama in Huntsville's Space Hardware Club, with the goal of developing and firing a small liquid rocket engine. To ensure the safe operation of the engine during firing and provide data to compare experimental data against, various modeling methods were applied to predict performance and structural responses during firing. For preliminary modeling, a quasi-1-dimensional model was developed in MATLAB to predict flow and performance parameters using a combination of standard compressible flow relations with chamber conditions coupled with mass flow rate. An additional 1-dimensional boundary layer cooling model is used to estimate the thermal performance of the fuel film cooling. Using values acquired with the 1-D analysis, structural and thermal FEAs were run within SolidWorks and MARC to show engine structural integrity for various proposed firing times. Additionally, to more accurately predict performance CFD simulations were run on the flow within the nozzle assuming equilibrium precombustion with frozen flow. Finally, CFD sims were set up to investigate injector flow and propellant impingement and the behavior of the fuel film coolants within the chamber.

## II. Engine Design

For its initial engine, the Tartarus project team has designed a small-scale liquid propellant engine dubbed "Prometheus." The current engine design includes a combustion chamber machined from 110 copper, with an unlike impinging doublet injector that will be machined from 304 stainless steel. The choice of these materials resulted from the pros each material presented when considering the environment they would need to withstand: 110 copper was chosen for the combustion chamber as the purity of this alloy results in high thermal conductivity and low reactivity with oxygen, and 304 stainless steel was chosen due to its similar coefficient of thermal expansion to the aforementioned 110 copper as well as its resistance to corrosion and ease of machining. Likewise, an unlike impinging

---

<sup>1</sup> Undergraduate, Mechanical and Aerospace Engineering Dept, amc010812@gmail.edu, Student Member, 1314313

<sup>2</sup> Undergraduate, Mechanical and Aerospace Engineering Dept, zdm0009@uah.edu, Student Member, 1422186

<sup>3</sup> Undergraduate, Mechanical and Aerospace Engineering Dept, cc0236@uah.edu, Student Member, 1605246

<sup>4</sup> Undergraduate, Mechanical and Aerospace Engineering Dept, tennis21player@gmail.com, Student Member, 1422186

<sup>5</sup> Undergraduate, Mechanical and Aerospace Engineering Dept, pgm0003@uah.edu, Student Member, 1604563

<sup>6</sup> Undergraduate, Mechanical and Aerospace Engineering Dept, jcw0060@uah.edu, Student Member, 1604662

doublet injector was chosen for its ease to manufacture and acceptable mixing characteristics with an impingement angle of 60 degrees.

Regarding the choice of propellants, many factors were considered in choosing what mixture of propellants would most efficiently fuel the engine. Liquid oxygen, while presenting difficulties in handling, was chosen as the oxidizer due to its overall high performance and reduced volatility and toxicity in comparison to other oxidizers. The chemical behaviors of both are also well documented. While non-denatured ethanol was originally considered due to its effectiveness as a coolant and ease of modeling, denatured ethanol was ultimately selected as it is safer to use and is more cost-effective while retaining cooling effectiveness. The selection of an effective coolant was vital as the team plans to use the method of fuel film cooling to cool the engine. Fuel film cooling involves diverting a small amount of the fuel flow to the walls of the engine chamber as a means of insulating the chamber walls from the extreme temperatures of combustion.

As for the scale of the design, the following table highlights some of the major dimensions of the current engine:

**Table 1: Prometheus Engine and Injector Geometry Parameters**

<b>Chamber Diameter</b>	3 inches	<b>Oxygen Orifice Diameter</b>	0.0512 inches
<b>Throat Diameter</b>	1 inch	<b>BLC Orifice Diameter</b>	0.0156 inches
<b>Chamber Length</b>	3 inches	<b>Fuel Orifice Angle</b>	52 degrees
<b>Expansion Angle</b>	15 degrees	<b>BLC Angle</b>	10 degrees
<b>Contraction Angle</b>	45 degrees	<b>Oxygen Injector Angle</b>	68 degrees
<b>Oxygen Orifice Diameter</b>	0.0512 inches	<b>Nozzle Expansion Ratio</b>	3

### III. 1-D Model

For initial modeling, a 1-D model was designed within MATLAB to calculate flow and performance parameters for engines of arbitrary injector properties, injector dimensions, propellants, and engine chamber dimensions. The simulation is designed to take a text file input specifying the aforementioned dimensions, as well as a chemical reaction file and output options. To solve the nonlinear system of equations describing chamber flow, a Gauss-Seidel method is employed. First, an initial guess for chamber pressure is made, set by default to 1 atm. Propellant flow rate into the chamber through each injector orifice is first calculated using the standard orifice flow equation, where  $\dot{m}$  is the mass flow rate through the orifice,  $C_d$  is the orifice coefficient of discharge,  $A$  is the orifice area,  $\rho$  is propellant density,  $p_0$  is manifold pressure, and  $p_c$  is the chamber pressure. Values for propellant density, among other required thermophysical or transport values, are calculated using the CoolProp property and equation-of-state calculator with its Matlab wrapper [2]. This calculation is repeated for each orifice and propellant manifold [1].

$$\dot{m} = C_d A \sqrt{2\rho(p_0 - p_c)} \quad (1)$$

Using this relation, a function for mass flow rate through each orifice based on chamber pressure is acquired for later solving, as each other variable is a constant of injector geometry or injector properties. This gives a new guess for chamber mass flow rate and propellant OF ratio.

$$OF = \frac{\dot{m}_{ox}}{\dot{m}_{fuel}} \quad (2)$$

With the OF ratio, the equilibrium combustion properties and products of the propellant mixture can be found using the open-source Cantera solver with its MATLAB wrapper [3]. Using the set command, a gas object using the designated chemical mechanism is created and set to the propellant temperatures, chamber pressure, and mass fraction of oxidizer and fuel according to the OF calculated previously. For a liquid propellant combination, an enthalpy correction must be applied to account for the heat of vaporization, as Cantera only models the gaseous phase. This is achieved by using the CoolProp plugin to find the enthalpy of the propellant mixture at injection temperature and subtracting it from a reference enthalpy in the gaseous phase (default evaluated at 600 K) to find an enthalpy difference between the two temperature points [2]. The Cantera gas object is set to the reference temperature, the enthalpy of the Cantera gas is extracted by command, and a new enthalpy is assigned by subtracting the CoolProp enthalpy difference

from the extracted Cantera enthalpy. Finally, combustion is evaluated by finding the chemical equilibrium of the fuel mixture at constant enthalpy and temperature.

$$h_{mix} = \frac{1}{OF+1} (h_{fuel}) + \frac{OF}{OF+1} (h_{ox}) \quad (3)$$

$$\Delta h_{corr} = h_{mix}(T_{ref}) - h_{mix}\left(\frac{1}{OF+1} T_{fuel} + \frac{OF}{OF+1} T_{ox}\right) \quad (4)$$

$$h = h_{Cantera}(T_{ref}) - \Delta h_{corr} \quad (5)$$

With Cantera, values of chamber temperature,  $T_c$ , ratio of specific heats,  $\gamma$ , and mean molecular weight,  $MW$ , can be extracted for the post-combustion mixture. Using these values and a guess for mass flow rate derived from Eq. (1), a new guess for chamber pressure can be found by an equation derived from Sutton [1].

$$p_c = \frac{\dot{m}}{A_t \gamma} \left( \frac{2}{\gamma+1} \right)^{\frac{\gamma+1}{\gamma-1}} \frac{-1}{\gamma R T_c} \quad (6)$$

With this value, a new guess for chamber pressure is obtained. Convergence criteria are evaluated by the relative error between iterations for chamber pressure and temperature, determining convergence when the maximum of these two errors is less than a default threshold of 1E-5. After convergence, the chamber values are used to calculate nozzle flow parameters according to standard compressible flow relations for a converging-diverging nozzle. First, a bisection zero-finding method is used to find the exit Mach number  $M_e$  based on the nozzle area ratio  $\frac{A_e}{A_t}$  and chamber ratio of specific heats  $\gamma$ .

$$M_e = \left( \frac{A_e}{A_t} \right)^{-1} \left( \frac{2}{\gamma+1} \right) \left( 1 + \frac{\gamma-1}{2} M_e^2 \right)^{\frac{\gamma+1}{2(\gamma-1)}} \quad (7)$$

With this, all of the required variables for the calculation of performance parameters are obtained and ready for processing. Exit pressure can be calculated with the exit Mach and ratio of specific heats. Next, the characteristic velocity  $c^*$ , a standard measure of combustion efficiency in a nozzle, is calculated, using the combustion gas parameters  $R$ , the post-combustion gas constant,  $\gamma$ , and  $T_c$ . An efficiency term,  $c^*_{eff}$ , is also applied to account for nozzle and combustion efficiency losses. Additionally, the coefficient of thrust,  $C_f$ , is calculated using  $\gamma$ , chamber pressure, chamber pressure  $p_c$ , exit pressure  $p_e$ , and ambient pressure  $p_a$ .

$$p_e = p_c \left( 1 + \frac{\gamma-1}{2} M_e^2 \right)^{-\frac{\gamma}{\gamma-1}} \quad (8)$$

$$c^* = \sqrt{\frac{RT_c}{\gamma} \left( \frac{\gamma+1}{2} \right)^{\frac{\gamma+1}{\gamma-1}}} \cdot c^*_{eff} \quad (9)$$

$$C_f = \sqrt{\left( \frac{2\gamma^2}{\gamma+1} \right) \left( \frac{2}{\gamma-1} \right)^{\frac{\gamma+1}{\gamma-1}} \left( 1 - \frac{p_e}{p_c} \right)^{\frac{\gamma-1}{\gamma}} + \frac{A_e}{A_t} \left( \frac{p_e}{p_c} - \frac{p_a}{p_c} \right)} \quad (10)$$

$$F = C_f \cdot c^* \cdot \dot{m} \quad (11)$$

$$I_{sp} = \frac{F}{9.81 \dot{m}} \quad (12)$$

After acquiring the necessary chamber parameters, the boundary layer cooling performance of the input engine is estimated according to the methods presented by Grissom in AEDC-TR-91-1 [4]. This consists of estimating the heat and momentum transfer from the chamber gases into the fuel film layer by correlations for the interfacial shear force, Reynolds, Prandtl, and Nusselt numbers, and thermal properties of the film. In addition to the convective heat transfer, radiative heat transfer is modeled through correlations for the emissivity of major combustion products H<sub>2</sub>O and CO<sub>2</sub>.

The thermal calculations are carried out in three phases: one where the film is below its saturation temperature and the thermal transfer heats up the fluid; another, when the film fluid is at its saturation temperature and evaporates at a rate defined by the fluid's latent heat of vaporization at flow pressure  $p$ , as evaluated by CoolProp according to Eq. (13); and a last phase, when the fluid film has fully evaporated, and heat transfer and insulation is dominated by entrainment of freestream gasses and expansion/contraction of the fluid gas layer with the nozzle.

$$LHV = h_{sat.gas}(p) - h_{sat.fluid}(p) \quad (13)$$

This fluid temperature is then assumed to be the wall temperature at steady state, assuming no more heat transfer. Additionally, in order to calculate the transient heat load into the walls, a heat transfer coefficient between the fluid and wall is calculated by the Bartz correlation taken from Sutton, using the coolant density  $\rho_{cool}$ , coolant velocity over the walls  $U_{cool}$ , chamber diameter at the evaluated point  $D$ , coolant ratio of specific heats  $\gamma_{cool}$ , coolant Prandtl number  $Pr_{cool}$ , and coolant dynamic viscosity  $\mu_{cool}$  [1].

$$h_{wall} = 0.023 (\rho_{cool} U_{cool})^{0.8} D^{-0.2} \gamma_{cool} Pr_{cool}^{0.4} \mu_{cool}^{-0.8} \quad (14)$$

For the current engine, the choice of propellants necessitated a chemical mechanism capable of simulating the combustion of ethanol with oxygen. To accomplish this, the PCRL mechanism by Roy et. al was chosen for its high fidelity and readily available reaction files [5]. With the current engine, the values taken from Table (1) and an assumed  $c^*$  efficiency of 90%, the following performance parameters were produced:

**Table 2: Estimated Performance Parameters for Prometheus Engine**

Chamber Temperature (K)	2091.48	Throat Steady-State Wall Temperature (K)	462.42
Chamber Pressure (PSI)	258.565	Fuel Mass Flow Rate (kg/s)	0.3132
Thrust (lbf)	251.15	Ox Mass Flow Rate (kg/s)	0.2853
ISP (s)	183.59	BLC Mass Flow Rate (kg/s)	0.0212
Coefficient of Thrust	1.3741	Combustion OF Ratio	0.911
Characteristic Velocity (m/s)	1358.43		

#### IV. Finite Element Structural Analysis - Injector

For the purposes of the project's simulation, mass flow rates of injected propellants as a function of manifold conditions and chamber pressure will be considered governed by the orifice flow equation as shown in Eq. (1). This will yield the mass flow rate through any given injector orifice as a function of ullage stagnation conditions and downstream chamber pressure.

To conduct a Finite Element Analysis on the injector, SolidWorks was used to do the thermal and structural analysis. For the meshing of the injector assembly, a curvature-based mesh was used because this was found to best preserve the geometry of the orifice holes [6]. For the thermal analysis, the first step was to find the heat transfer convection coefficients,  $h$ , for the flowing propellants and the ignitor. To do this, the specific heat at constant pressure, dynamic viscosity, density, and thermal conductivity for ethanol at 350 psi and 290 K and oxygen at 350 psi and 85 K are looked up through CoolProp [2]. With the dimensions of the injector, the velocity of the propellants through the injector and orifice holes is found using Eq. (15) below where  $A$  is the area of the hole and  $\dot{m}$  is the mass flow rate through the hole.

$$v = \frac{\dot{m}}{\rho A} \quad (15)$$

With the velocity through the injector holes, the Reynolds number for the holes can be found using Eq. (16) below, where the characteristic length  $L$  is the diameter of the hole and  $\mu$  is the dynamic viscosity of the flowing propellant [7].

$$Re_D = \frac{\rho v L}{\mu} \quad (16)$$

Next, the Prandtl's number for each propellant is determined using Eq. (17) below where  $k$  is the thermal conductivity and  $C_p$  is the specific heat at constant pressure [7].

$$Pr = \frac{\mu C_p}{k} \quad (17)$$

The convective heat transfer coefficient for the propellants flowing through the injector is found in Eq. (18) below, where  $Nu_D$  is the Nusselt number. To find the Nusselt number, Eq. (19) is used, where  $f$  is the Darcy friction factor, which is obtained in Eq. (20) below [7].

$$h = \frac{Nu_D k}{L} \quad (18)$$

$$Nu_D = \frac{(f/8)(Re_D - 1000)Pr}{1 + 12.7(f/8)^{1/2}(Pr^{2/3} - 1)} \quad (19)$$

$$f = (0.79 \ln(Re_D) - 1.64)^{-2} \quad (20)$$

Once the convective heat transfer coefficients are found, the next step is to conduct a thermal study of the ignitor firing for 2 seconds before ignition. For this thermal study and every subsequent one, the exterior faces of the injector would be exposed to air at 290 K, which would transfer heat at a rate of  $12.12 \frac{W}{m^2 K}$ , and the component interaction is treated as bonded [6] [8]. In this study, conducted over a 2-second interval with timesteps of 0.25 seconds, the convective heat transfer from the ignitor, calculated with the equations mentioned earlier, is applied to the injector. The results of the thermal study are below in Figure (1).

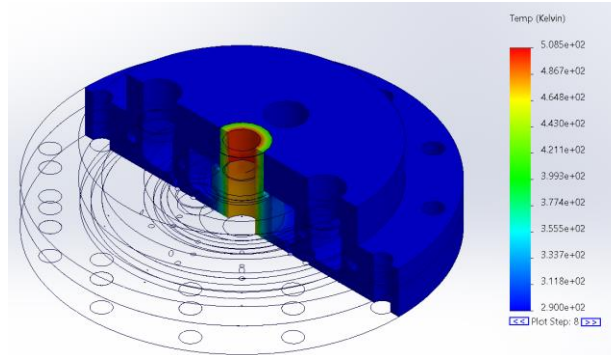


**Figure 1: Thermal study for ignitor firing after 2 seconds**

Next, a thermal study is conducted with the initial temperatures imported from the end of the previous study for the first 3 seconds of engine firing with timesteps of 0.25 seconds, in which the ignitor will be running in addition to having the propellants flowing through the injector. As with the previous study, the convective heat transfer from the ignitor is applied to the injector. In addition, radiative heat transfer from the combustion chamber is applied on the bottom of the injector with an ambient temperature of 2000 K, a source emissivity of 0.4665 as calculated through the radiative heat transfer method in AEDC-TR-91-1, a view factor of 0.5, and the convective heat transfer coefficients calculated earlier are applied to the oxidizer, ethanol, and BLC orifices and manifolds [4]. After this study is conducted, a final thermal study is conducted during the last 7 seconds of engine firing, which has the same conditions as the previous study except the heat transfer from the ignitor is no longer applied. The results from these thermal studies are shown in Figure (2).

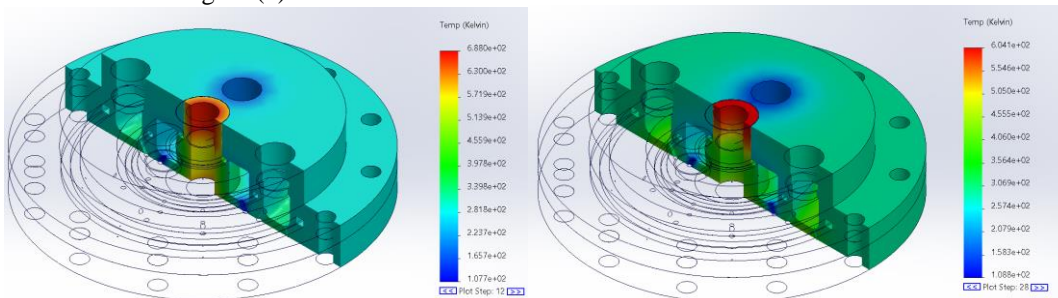


**Figure 2: Thermal study for engine firing at 3 and 10 seconds after engine ignition**

With the results from the thermal study in Figure (2), a structural analysis of the injector after 10 seconds of firing was conducted through a static study in SolidWorks. For the static study, the bolt holes on the injector and the bottom section not exposed to the engine chamber were designated as fixed geometries, bolt connections torqued to 8 lbf-ft, the tightness specification for the bolts we are using [9-10], were added to the bolt holes in the injector, and the component interaction was set to contact for the injector assembly [6]. For the loads applied on the injector, the thermal effects from the end of the thermal study in Figure (2) were imported and applied, a pressure of 250 psi was applied to the bottom of the injector, and a pressure of 350 psi was applied to the manifolds and orifices of the injector. The graph for the Von Mises Stress after 10 seconds is shown below in Figure (3), while the FOS Graph, taken with respect to the ultimate strength of the material, is also shown.

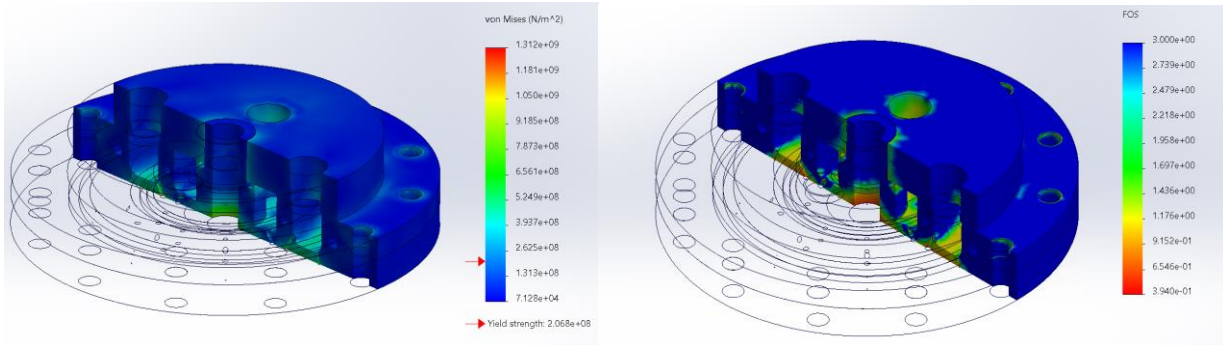
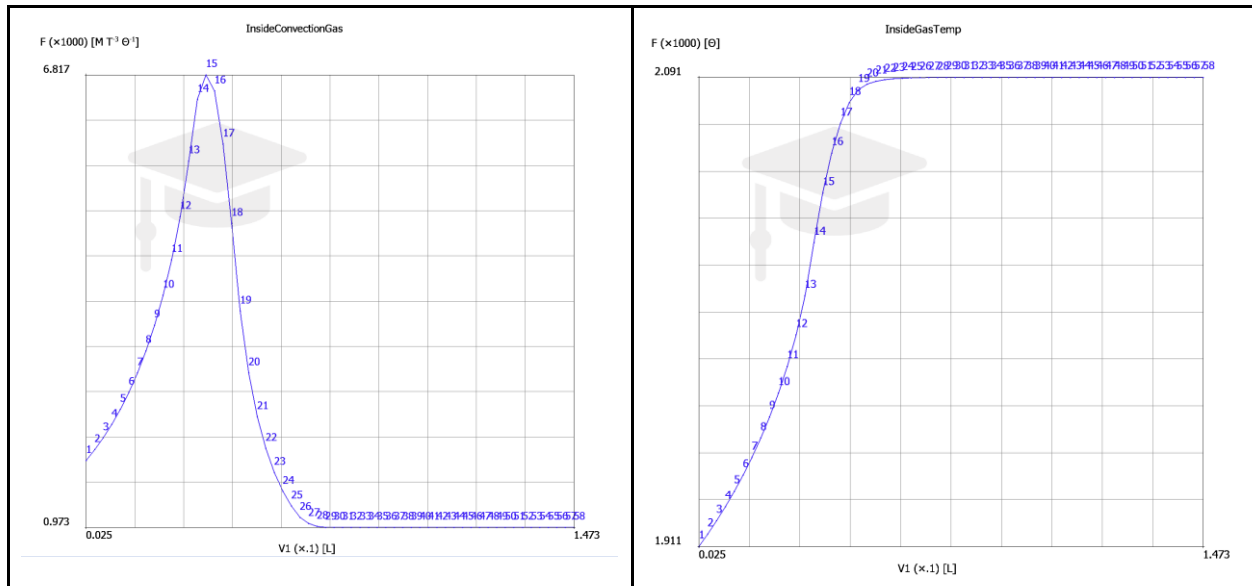


**Figure 3: Von Mises Stress and FOS plot 10 seconds After Engine Ignition**

The results of the structural analysis show that the bottom of the injector will be subjected to stresses that exceed the ultimate tensile strength of 304 stainless steel due to the shear thermal gradient between the bottom of the injector and the bottom of the propellant manifolds. With future CFD results, the heat transfer assumptions will be improved for further analysis to better estimate the severity of this issue; if the problem is corroborated by further analysis, the injector may be redesigned to have a thinner bottom to possibly reduce thermal gradient stress.

### V. Finite Element Structural Analysis - Engine Chamber

Using the heat transfer coefficients calculated in the MATLAB models with Eq. (14), thermal and structural studies for the engine chamber can be run in MSC Marc [11]. The first important step is to make sure that the data was correct for where they correlate in axial alignment. With the x-axis starting at the exit of the engine chamber, the following were the charts that studies used for the thermal studies.



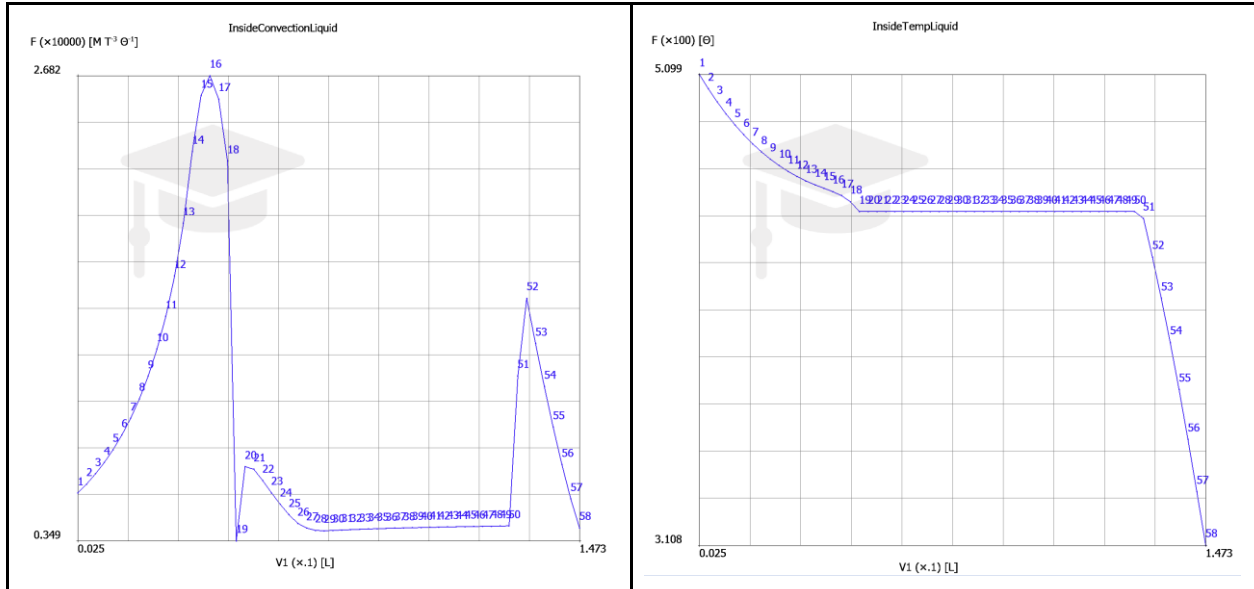


**Figure 4: Charts from MSC Marc used for Thermal Studies**

With those thermodynamic values, transient studies can be performed. Since the engine chamber will be outside in standard atmospheric conditions, an initial temperature of 295 K is used. To establish bounds on expected wall heating, simulations with and without film cooling were set up to represent the expected and worst-case scenarios, respectively. To set up the study without film cooling, the tables with the gas coefficient of convection and the temperature of the gas in the chamber are used, with heat transfer from the hot gas calculated via Bartz correlation in Eq. (14) [1]. This is used to establish a forced-convection heat transfer boundary for the chamber interior. For the exterior, a heat transfer boundary is set with a convection coefficient of 25 W/m-K and an ambient temperature of 295 Kelvin to represent the free convection of air. The transient study runs for 10 seconds to represent the max expected firing time. The next study to perform is the thermal study of the engine chamber with film cooling performing exactly how the models expect it to. To accomplish this, the heat transfer coefficient of the ethanol coolant from Eq. (14) on the chamber walls and the temperature of the coolant is used to apply an internal heat transfer boundary. This boundary condition was set along the axial length of the inside of the engine chamber. The same exterior free-convection boundary conditions as the other study is used. This transient study is also run for 10 seconds for max firing time.

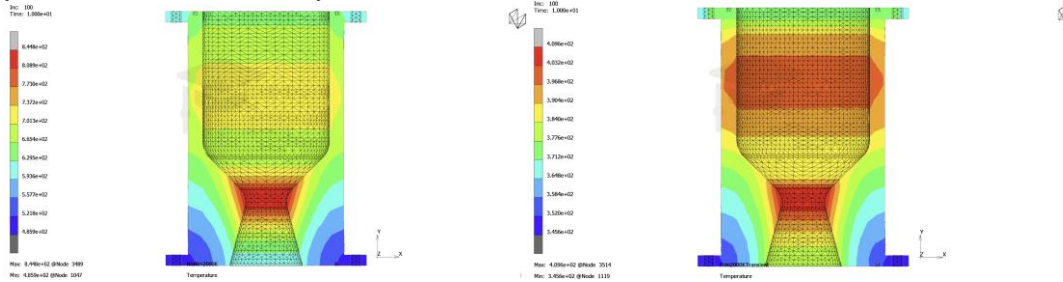


**Figure 5: Thermal Study of Engine Chamber Without Film Cooling vs with Film Cooling at 10 seconds**

Next, structural stress structures are run to evaluate the engine’s structural integrity during firing. Using the MATLAB model and the compressible flow equations, local flow pressure as a function of Mach number is obtained [1]. The pressure is plotted for Marc to use along the axial distance of the chamber.

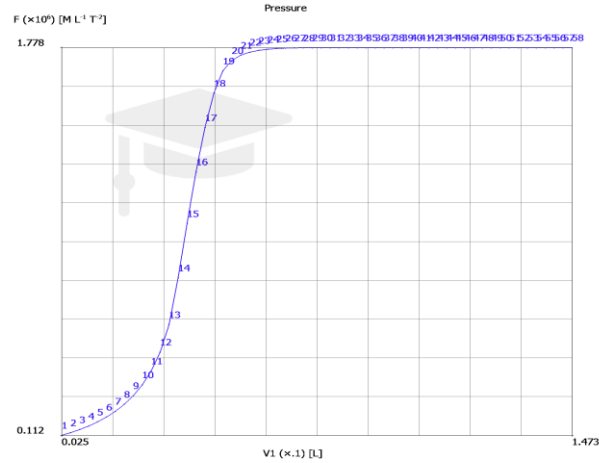


**Figure 6: Pressure along the axial length of the engine chamber**

This data is used for the boundary condition on the inside of the chamber and the standard atmospheric pressure of 101325 Pa is used for the outside of the chamber. The chamber will be held in place by bolts, so a fixed displacement condition is used to allow for the chamber to be held in place for the study to be performed. Also, to account for the thermal stresses of the chamber, the temperature data from the previous studies is applied in conjunction with the structural study. The study for the chamber without the film cooling was the first to be analyzed with Von Mises Stress. The same study can be done with the temperature data from the study with film cooling and a comparison of the two results can be made.

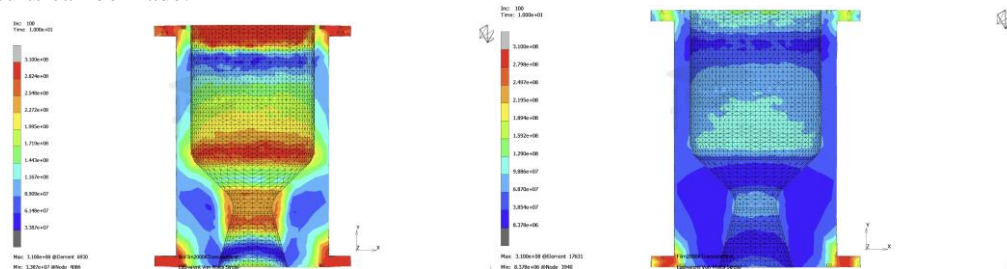


**Figure 7: Von Mises Stress plot of no film cooling vs with film cooling at 10 seconds**

The results show that the engine chamber experiences more stress concentrations when there is no film cooling, but there is to be yielding at the flange on the bottom as those experience the greatest amount of displacement due to thermal loads.

## VI. Computational Fluid Simulations - Nozzle

To further validate engine performance, a CFD simulation of the engine nozzle was designed and run. OpenFOAM was chosen for this application primarily because it is open source, versatile, and efficient, in addition to the possibility of its text file inputs being written by the 1-D MATLAB model. The first challenge that needed to be addressed was the need for a usable mesh. MATLAB, along with OpenFOAM's built-in blockMesh function, generates a section of our combustion chamber and nozzle spanning 2 degrees of the engine; this allows for axisymmetric simulations to be performed as the mesh can be made one cell thick. Because of the 2-D nature of the simulation, significantly fewer computational resources are required, which makes it possible to run these simulations as a student group with minimal computational resources. This mesh file was written by a MATLAB subroutine run alongside the performance sim which built the engine geometry based on the geometry parameters input into the simulation. Prism cells were applied to the wall boundaries of the chamber slice to improve the resolution of boundary layer effects and near-wall turbulence.

For this initial simulation, a frozen flow model was created, in which a pre-combusted mixture according to the chemical equilibrium calculated in the 1-D MATLAB simulation is injected at an inlet comprising the top plane of the engine geometry, progressing through the nozzle before reaching the outlet boundary condition. Turbulence in the flow is modeled according to the k-omega SST model, owing to its better resolution of near-wall turbulence behavior and blending function allowing for accurate and efficient turbulence modeling in both near-wall and freestream

conditions [12]. Thermodynamic and transport variables are set to constants based on the 1-D combustion products, with values averaged over the expected temperature range. Numerical schemes are generally set to linear options, with a limited linear option used for most divergence terms, which blends between linear and upstream discretization methods based on local gradient change [13]. For timestep discretization, a local Euler time step method is used, which applies a local timestep to each cell based on flow conditions, allowing the flow to accelerate towards steady-state convergence faster than traditional transient methods with greater stability than a steady-state discretization.

Boundary conditions are assigned according to Table (4), with inlet flow being mass-flow driven with a fixed combustion temperature. The simulation is run for 10,000 iterations, with a final global continuity residual on the order of  $10^{-11}$ . Final data processing and visualization takes place with Paraview, with axial values extracted along the axis of symmetry.

**Table 4: Boundary Conditions of Frozen Flow Simulation**

	Velocity	Pressure	Temperature	Specific Turbulent Dispersion ( $\omega$ )	Turbulent Kinetic Energy (k)	Turbulent Viscosity	Turbulent Thermal Diffusivity
<b>Inlet</b>	flowRateInlet Velocity	zeroGradient	fixedValue	fixedValue	fixedValue	calculated	calculated
<b>Outlet</b>	zeroGradient	zeroGradient	zeroGradient	inletOutlet	inletOutlet	calculated	calculated
<b>Walls</b>	noSlip	zeroGradient	zeroGradient	omegaWall Function	kqRWallFunction	nutkWallFunction	compressible::alphaWall Function
<b>Axis Boundaries</b>	wedge	wedge	wedge	wedge	wedge	wedge	wedge

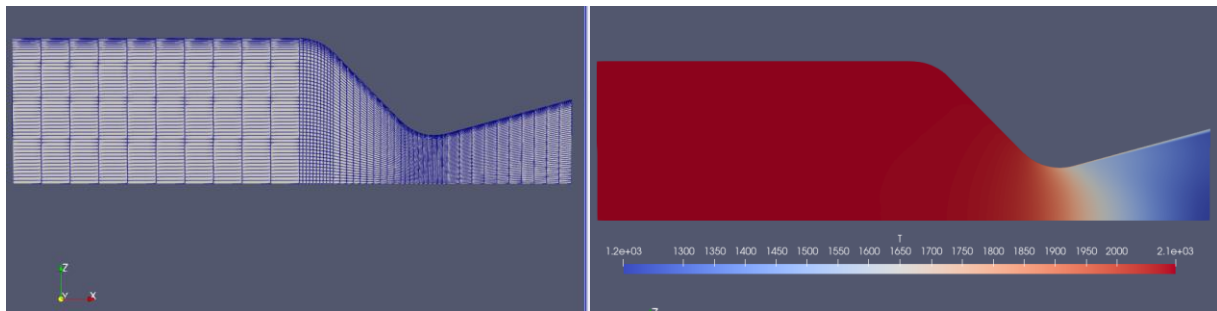


**Figure 8: View of Engine Mesh and Steady-State Temperature Contour**

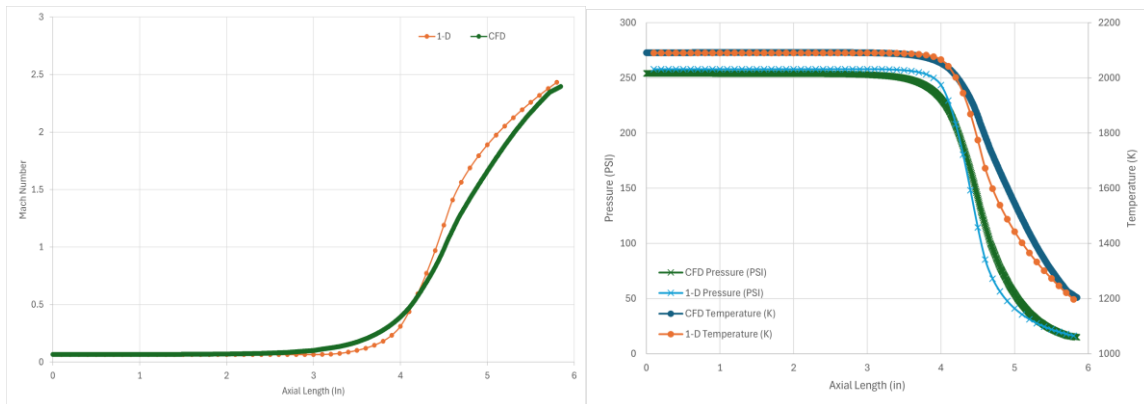


**Figure 9: Comparison Between 1-D and CFD Flow Values along Chamber Axis**

After convergence, the CFD predicts a chamber pressure of 253.924 psi, for a relative percent error compared to 1-D of 1.5%. As shown in Fig. (9), critical flow values for the 1-D and CFD sims match reasonably well, with the CFD showing more gradual gradients than the 1-D, likely due to non-ideal flow assumptions and greater influence of surrounding flow conditions. Using the surface integrate function in Paraview, the thrust is calculated to be 267.84 lbf, 6.6% higher than our 1-D estimate and corresponding to a  $c^*$  efficiency of 96%, much better than the previous 90%; while this does not account for combustion and mixture efficiency, this suggests that actual engine performance is higher than current predictions and serves as a measure of nozzle efficiency.

For higher-fidelity simulation of conditions within the nozzle, a reacting-flow simulation is being developed to account for transient reactions within the nozzle. This would better simulate flow within the nozzle during firing, as it would both account for changing fluid thermodynamic and transport variables along with the potential heat absorbed or released by these reactions, affecting performance. Such a simulation would be set up identically to the prior, with additional boundary condition definitions at the inlet to fix the mass fractions of each simulated component to the composition predicted by Cantera and the PCRL mechanism in the 1-D simulation [5]. The PCRL mechanism Chemkin files would additionally be imported into OpenFOAM to provide reaction information for the simulation. With this, the team aims to predict nozzle effectiveness more accurately by accounting for nozzle reactions.

## VII. Computational Fluid Simulations - Injector and BLC Flow Simulation

In addition, to model the effectiveness of the injector manifold in fuel mixing and BLC injection, another coupled multiphase sim is being developed to model the behavior of the injection. Within ANSYS, a mesh was built representing the internals of the fuel and oxidizer manifolds and the top portion of the engine chamber, cut into  $\frac{1}{4}$  slices to take advantage of symmetrical geometry and reduce computational costs. This model is then imported into OpenFOAM using the `fluentMeshToFoam` command. To model the stratified multiphase flow of the liquid fuels and air, the Volume-of-Fluids model is used with an interface compression scheme to model sharp stratification between the gas and liquid phase [12]. A coupled fluid film simulation will also be used to simulate the flow of the BLC along the engine walls along with a VOF-to-film transition module to calculate the deposition of BLC on the engine walls from the injector. With this model, more accurate values for injector manifold heat transfer may be obtained, alongside qualitative studies of the propellant injection and mixing behavior and BLC wall coverage.

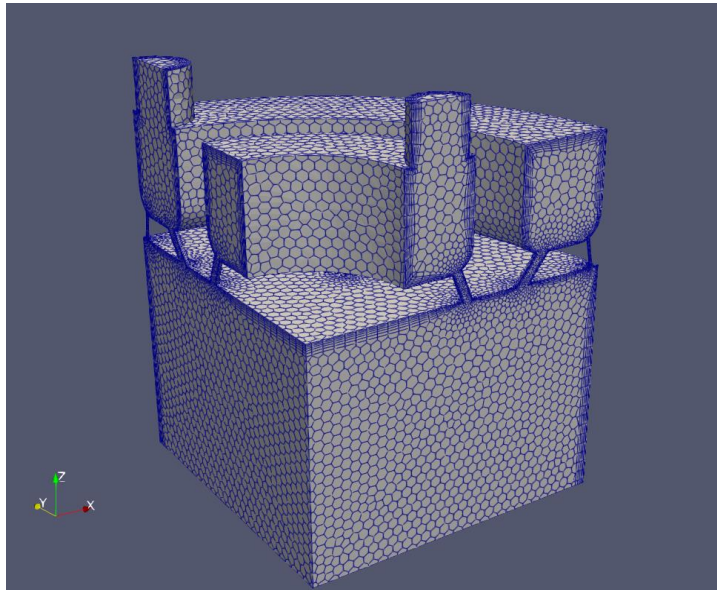


**Figure 10: Isometric View of Injector Manifold Mesh**

## VIII. Conclusion

Moving forward, the Tartarus team plans to continue developing higher fidelity models such that we can verify the Prometheus engine's design safety and performance parameters. With our current modeling techniques, the team is progressing towards more informed and improved designs and more accurate and reliable performance predictions. Through the improvement of these models and modeling techniques, along with the data gathered from hot fire, the team will be able to build models and simulations accurate and reliable enough to further drive design decisions and

enable the construction of more ambitious and higher-performing rocket engines, culminating in the creation of a high-fidelity digital twin model of the entire engine system to supplement physical testing. Additionally, the team hopes to increase the breadth of knowledge surrounding amateur liquid rocketry to enable more teams to do this work.

## IX. Acknowledgments

The authors would first and foremost like to thank Dr. Gang Wang for his mentorship to The University of Alabama in Huntsville's Space Hardware Club, as well as Dr. Xu for representing AIAA at The University of Alabama in Huntsville. The team are also very grateful to the MAE department at UAH and Mr. Jon Buckley in particular for the use of their machine shop. The Alabama Space Grant Consortium and the University of Alabama in Huntsville have graciously given us the resources necessary to fund this project through the Space Hardware Club. Finally, we would like to thank all members of Tartarus for their continued support and dedication to the project, as well as alumni Jack Slayden and Sean Rabbitte, whose prior efforts laid much of the groundwork for the recent work described.

## X. References

- [1] Sutton, G. P., and Biblarz, O., *Rocket Propulsion Elements*, Hoboken, NJ: John Wiley & Sons, Inc, 2017.
- [2] Bell, H. I., Wronski, J., Quoilin, S., and Lemort, V., "Pure and Pseudo-pure Fluid Thermophysical Property Evaluation and the Open-Source Thermophysical Property Library CoolProp," *Industrial & Engineering Chemistry Research*, Vol 53, No. 6, 2014, pp. 2498-2508, DOI: 10.1021/ie4033999
- [3] David G. Goodwin, Harry K. Moffat, Ingmar Schoegl, Raymond L. Speth, and Bryan W. Weber. Cantera: An object-oriented software toolkit for chemical kinetics, thermodynamics, and transport processes. <https://www.cantera.org>, 2023. Version 3.0.0. doi:10.5281/zenodo.813709
- [4] Grissom, W. M., "Liquid Film Cooling in Rocket Engines," Air Force AEDC-TR-91-1, March 1991.
- [5] Roy, R. Mishra, O. Askari, et al., "Reduced ethanol skeleton mechanism for multidimensional engine simulation," *Journal of the Energy Institute*, Vol 106, Feb. 2023
- [6] SolidWorks, Ver 2022 SP03.1 Student Edition, Dassault Systems, 2024.
- [7] Incropera, F. P., DeWitt, and David P., *Fundamentals of Heat and Mass Transfer* (6th ed.). Hoboken, NJ: John Wiley & Sons, Inc, 2007.
- [8] The Engineering ToolBox (2003), Convective Heat Transfer. [https://www.engineeringtoolbox.com/convective-heat-transfer-d\\_430.html](https://www.engineeringtoolbox.com/convective-heat-transfer-d_430.html). Accessed Feb. 24, 2024
- [9] McMaster-Carr, Medium-Strength Steel Hex Nut, Grade 5, 1/4"-20 Thread Size. <https://www.mcmaster.com/95505A601/>. Accessed Feb. 24, 2024
- [10] Alma Bolt Company & Prime Fasteners, Tightening Torque Guide. <https://www.almabolt.com/pages/catalog/bolts/tighteningtorque.htm>. Accessed Feb. 24, 2024
- [11] Marc, MSC Marc and Mentat, Software Package, Ver 2023.1 Student Edition, Hexagon AB, 2024.
- [12] Strelnikov G, Pryadko N\*, Ihnatiev O and Ternova K. "Choice of a Turbulence Model for Modeling Complex Flows in Rocket Engine Nozzles." *Nov Res Sci*. 11(1). NRS. 000751. 2022. DOI: 10.31031/NRS.2022.10.000751
- [13] Greenshields, Christopher. OpenFOAM v11 User Guide. The OpenFOAM Foundation, 2023.